

This is an Open Access document downloaded from ORCA, Cardiff University's institutional repository: <https://orca.cardiff.ac.uk/id/eprint/132899/>

This is the author's version of a work that was submitted to / accepted for publication.

Citation for final published version:

Mead, Ben , Cullather, Erin, Nakaya, Naoki, Niu, Yuzhe, Kole, Christo, Ahmed, Zubair and Tomarev, Stanislav 2020. Viral delivery of multiple miRNA promotes retinal ganglion cell survival and functional preservation after optic nerve crush injury. *Experimental Eye Research* 197 , 108071. 10.1016/j.exer.2020.108071

Publishers page: <http://dx.doi.org/10.1016/j.exer.2020.108071>

Please note:

Changes made as a result of publishing processes such as copy-editing, formatting and page numbers may not be reflected in this version. For the definitive version of this publication, please refer to the published source. You are advised to consult the publisher's version if you wish to cite this paper.

This version is being made available in accordance with publisher policies. See <http://orca.cf.ac.uk/policies.html> for usage policies. Copyright and moral rights for publications made available in ORCA are retained by the copyright holders.



1 **Viral Delivery of Multiple miRNA Promotes Retinal Ganglion Cell**
2 **Survival and Functional Preservation after Optic Nerve Crush**
3 **Injury**

4 Ben Mead^{a, b, *}, Erin Cullather^b, Naoki Nakaya^b, Yuzhe Niu^b, Christo Kole^b, Zubair Ahmed^{c, 2},
5 Stanislav Tomarev^{b, 2*}

6 ^a School of Optometry and Vision Sciences, Cardiff University, Cardiff, UK, CF24 4HQ

7 ^b Section of Retinal Ganglion Cell Biology, Laboratory of Retinal Cell and Molecular Biology,
8 National Eye Institute, National Institutes of Health, Bethesda, Maryland, 20892, USA

9 ^c Neuroscience and Ophthalmology, Institute of Inflammation and Ageing, University of
10 Birmingham, Birmingham, B15 2TT, UK

11

12 ² Joint senior authors

13 *Corresponding authors at: MeadB@Cardiff.ac.uk; tomarevs@nei.nih.gov

14

15 Author contributions:

16 B.M: Designed the experiment; Conducted the experiment; Analysed/interpreted data; Wrote the
17 article, Proofed/revised article

18 E.C: Conducted the experiment

19 N.N: Conducted the experiment

20 Y.N: Conducted the experiment

21 C.K: Conducted the experiment

22 Z.A: Designed the experiment, Proofed/revised article

23 S.T: Designed the experiment; Analysed/interpreted data; Proofed/revised article

24 **Running title:** miRNA-mediated RGC neuroprotection

25 **Key words:** Retinal ganglion cells, miRNA, Optic nerve crush, Exosomes, PTEN, Adeno-
26 associated virus, neuroprotection,

27

28 **Abstract**

29 Bone marrow mesenchymal stem cell (BMSC)-derived small extracellular vesicles (sEV) but not
30 fibroblast sEV provide retinal ganglion cell (RGC) neuroprotection both *in vitro* and *in vivo*,
31 with miRNAs playing an essential role. More than 40 miRNAs were more abundant in BMSC-
32 sEV than in fibroblast-sEV. The purpose of this study was to test the *in vitro* and *in vivo*
33 neuroprotective and axogenic properties of six candidate miRNAs (miR-26a, miR-17, miR-30c-
34 2, miR-92a, miR-292, and miR-182) that were more abundant in BMSC-sEV than in fibroblast-
35 sEV. Adeno-associated virus (AAV)-2 expressing a combination of three of the above candidate
36 miRNAs were added to heterogenous adult rat retinal cultures or intravitreally injected into rat
37 eyes one week before optic nerve crush (ONC) injury. Survival and neuritogenesis of β III-
38 tubulin⁺ RGCs was assessed *in vitro*, as well as the survival of RBPMS⁺ RGCs and regeneration
39 of their axons *in vivo*. Retinal nerve fiber layer thickness (RNFL) was measured to assess axonal
40 density whereas positive scotopic threshold response electroretinography amplitudes provided a
41 readout of RGC function. Qualitative retinal expression of PTEN, a target of several of the above
42 miRNAs, was used to confirm successful miRNA activity. AAV2 reliably transduced RGCs *in*
43 *vitro* and *in vivo*. Viral delivery of miRNAs *in vitro* showed a trend towards neuroprotection but
44 remained insignificant. Delivery of selected combinations of miRNAs (miR-17-5p, miR-30c-2
45 and miR-92a; miR-92a, miR-292 and miR-182) before ONC provided significant therapeutic

46 benefits according to the above measurable endpoints. However, no single miRNA appeared to
47 be responsible for the effects observed, whilst positive effects observed appeared to coincide
48 with successful qualitative reduction in PTEN immunofluorescence in the retina. Viral delivery
49 of miRNAs provides a possible neuroprotective strategy for injured RGCs that is conducive to
50 therapeutic manipulation.

51 **1. Introduction**

52 Neurons of the mammalian central nervous system (CNS) suffer from an intrinsic inability to
53 regenerate their axons after injury, a characteristic that underpins the associated functional
54 deficits. Due to the diencephalic origin of the optic vesicles during development, the retina is
55 considered an outgrowth of the brain and thus, a CNS structure. Retinal ganglion cells (RGCs)
56 are the final stage in the phototransductive pathway and their axons make up the optic nerve.
57 Damage to the optic nerve may lead to irreversible blindness and is often used not just as a
58 model for traumatic optic neuropathy but also for spinal cord injury.

59 Delivery of neurotrophic factors (NTF) has proven inefficient in promoting long-term
60 neuroprotection, likely because of two reasons: (1), the need for frequent administration and in
61 combination; and (2), the subsequent down-regulation of their receptors after treatment. Delivery
62 of cells, those that release NTF naturally (Johnson et al., 2010; Mead et al., 2016; Mead et al.,
63 2013) or those that have been modified to release glial cell line-derived neurotrophic factor and
64 ciliary neurotrophic factor (Flachsbarth et al., 2018) addresses the longevity issue. In contrast, to
65 address the receptor down-regulation problem, delivery of a virus to induce the expression of
66 both brain-derived neurotrophic factor and its receptor TrkB in RGCs promotes neuroprotection
67 after ONC and laser-induced glaucoma (Osborne et al., 2018). We recently demonstrated that
68 cell therapy, namely bone marrow mesenchymal stem cells (BMSC), are effective at protecting

69 RGCs from death *via* the exosomes/small extracellular vesicles (sEV) they secrete and in
70 particular, the microRNAs (miRNAs) contained within (Mead et al., 2018; Mead and Tomarev,
71 2017).

72 miRNAs are short non-coding RNA that mediate the knockdown and silencing of mRNA *via* the
73 guiding of Argonaute (AGO) proteins to target sites complementary to the miRNA sequence
74 (Reviewed in Gebert and MacRae, 2018). Approximately 2500 miRNAs have been identified in
75 humans and their importance is underpinned by the lethality of Dicer/Drosha knockout. Drosha
76 is necessary for the conversion of pri-miRNA to pre-miRNA whereas Dicer cleaves the pre-
77 miRNA into mature miRNA ready for loading into the AGO complex. The most highly
78 expressed of the AGO proteins is AGO2 and is considered the integral component of the RNA-
79 induced silencing complex (Liu et al., 2004). Knockdown of AGO2 perturbs the neuroprotective
80 and neuritogenic efficacy of BMSC exosomes on injured RGCs (Mead et al., 2018; Mead and
81 Tomarev, 2017; Zhang et al., 2016).

82 Deviations in the expression of miRNA have been associated with several neurodegenerative
83 diseases including Parkinson's, Huntington's and Alzheimer's disease (Reviewed in Rajgor,
84 2018). For example, in amyotrophic lateral sclerosis, release of miR-218 from motor neurons can
85 disrupt the function of nearby astrocytes and contribute to the disease pathology (Hoye et al.,
86 2018). In experimental autoimmune encephalomyelitis, lumbar motor neurons and retinal
87 neurons displayed a differential expression of 14 miRNA in comparison to healthy animals
88 (Juźwik et al., 2018).

89 While miRNAs downregulate mRNA and thus subsequently the encoded proteins, the overall
90 effect can still be an activation of discrete signalling pathways. One relevant example in the field
91 of axon regeneration is phosphatase and tensin homolog (PTEN), a suppressor of the pro-

92 regenerative mTOR/PI3K/Akt pathway. PTEN knockdown promotes axon regeneration in the
93 CNS (Reviewed in Berry et al., 2016). Several miRNAs have been found to target PTEN and
94 subsequently activate the mTOR pathway including miR-214 (Bera et al., 2017), miR-1908 (Xia
95 et al., 2015), miR-494 (Wang et al., 2010) and miR-21 (Sayed et al., 2010). Indeed exosomes
96 derived from MSC promote regeneration of cortical neurons *via* activation of the mTOR
97 pathway (Zhang et al., 2016). In a model of glaucoma, inhibitors of miR-149 were shown to be
98 RGC neuroprotective along with an associated upregulation of the PI3K/Akt pathway (Nie et al.,
99 2018). Delivery of miRNA *via* Schwann cell-derived exosomes into cultured neurons promoted
100 neuritogenesis, evident by the lack of effect if exosomes were ablated of RNA (Ching et al.,
101 2018). Candidate miRNAs included miR-21, miR-222, miR18a and miR182.

102 In the present study we expressed combinations of six candidate miRNAs (miR-26a, miR-17,
103 miR-30c-2, miR92a, miR-292, and miR-182) using self-complimentary adeno-associated virus
104 (AAV)-2 in the RGCs of rats that have undergone a crush injury to the optic nerve and assessed
105 survival, regeneration and functional preservation. These candidates were chosen based on their
106 abundance in the neuroprotective BMSC-derived sEV in comparison to the ineffective
107 fibroblast-derived sEV.

108 **2. Materials and Methods**

109 All reagents were purchased from Sigma (Allentown, PA) unless otherwise specified.

110 **2.1 Animals**

111 Adult female Sprague-Dawley rats weighing 200-220 g (Charles River, Wilmington, MA) were
112 maintained in accordance with guidelines described in the ARVO Statement for the Use of

113 Animals in Ophthalmic and Vision Research, using protocols approved by the National Eye
114 Institute Committee on the Use and Care of Animals.

115 Animals were kept at 21°C and 55% humidity under a 12 hours light and dark cycle, given
116 food/water *ad libitum* and were under constant supervision from trained staff. Animals were
117 euthanized by rising concentrations of CO₂ before extraction of retinae.

118 **2.2 Plasmid and AAV production**

119 Backbone for all miRNA constructs is the pscAAV-CMV-ΔelD, modified plasmid used in a
120 previous publication (Kole et al., 2018) but lacking the D-element in 3' ITR sequence. Cassette of
121 EmGFPmiR_NegControl (Thermo Fisher Scientific, Cincinnati, OH; #K4936-00) was subcloned
122 into pscAAV-CMV -ΔelD using Gateway® recombination reactions. miRNA loci tested (**Table**
123 **1**) were obtained from miRBase <http://mirbase.org/>. Individual loci containing a single miRNA
124 stem-loop were generated as PCR primers containing a complementary single-stranded DNA
125 sequence and extended via high-fidelity PCR as one cycle of 15 seconds at 95°C followed by
126 annealing for 15sec at 62°C and extension at 72°C for 15 sec. Double stranded sequences were
127 subcloned using restriction enzymes SalI and EcoRV into pscAAV-CMV-
128 EmGFPmiR_NegControl-ΔelD vector by replacing the miR_NegControl sequence. Each
129 miRNA sequence was validated by sequencing analysis. Self-complementary AAV production
130 were generated as described (Kole et al., 2018). Importantly, self-complementary AAV vectors
131 induce replication/translation much faster (2 days) than conventional AAV vectors (4 weeks).
132 While conventional AAV vectors require the host cell to synthesize the second complementary
133 strand from its palindromic inverted terminal repeats, self-complementary AAV vectors include
134 this second strand and thus ignore this rather significant rate-limiting step (McCarty, 2008).
135 Briefly, HEK 293T cells were triple transduced with pHelper, pAAV2cap, and pscAAV2-CMV-

136 (GFPmiRNA) plasmids using polyethylenimine. For increasing the screening scale, each viral
137 batch contained the combinations of three different pscAAV2-CMV-(GFPmiRNA) constructs
138 and are referred to as virus collection A-E in **Table 2**. The iso-molar combination of plasmids is
139 expected to generate same number of viral particles of each GFPmiRNA. Cells were harvested
140 48 h after transduction. Viral particles were purified by centrifugation through iodixanol gradient
141 (15, 25, 40, and 60%). The 40% fraction containing the AAV viral particles was collected and
142 passed through the column for desalting. Viral particles were suspended and stored in phosphate-
143 buffered saline (PBS), 0.001% pluronic (Thermo Fisher Scientific; #24040) which prevents
144 attachment of virus to pipette or tube. Titers (viral genomes per ml - vg/ml) were determined by
145 real time PCR using the primers targeting the CMV promoter: 5'-
146 ATGCGGTTTTGGCAGTACAT-3' and 5'-GTCAATGGGGTGGAGACTTG-3'.

147 **2.3 Adult rat retinal cell culture**

148 Eight-well chamber slides (Thermo Fisher Scientific) were pre-coated with 100 µg/ml poly-D-
149 lysine/20 µg/ml laminin for 60/30 minutes respectively. After culling and ocular dissection,
150 retinal cells were dissociated into single cells using a Papain Dissociation system according to
151 the manufacturer's instructions (Worthington Biochem, Lakewood, NJ) and as described
152 previously (Logan et al., 2006). Retinal cells were seeded at 125,000 cells/well in 8-well
153 chamber slides and grown in 300µl of supplemented Neurobasal-A (25 ml Neurobasal-A
154 (Thermo Fisher Scientific), 1X concentration of B27 supplement (Thermo Fisher Scientific), 0.5
155 mM of L-glutamine (62.5 µl; Thermo Fisher Scientific) and 50 µg/ml of gentamycin (125 µl;
156 Thermo Fisher Scientific)). Cultures were treated with virus collection A, B, C, D, or E which
157 contained 1×10^{11} vg/ml in sterile PBS, 0.001% pluronic in a final volume of 5 µl (**Table 2**). All

158 *in vitro* experiments were run in triplicate from pooled retinae from 2 animals and repeated on
159 three independent occasions (total of 6 separate animals).

160 Cultures were incubated for 3 days at 37°C before immunocytochemical staining of RGCs with
161 β III-tubulin to stain cell soma and neurites (Logan et al., 2006). For this study, large spherical
162 β III-tubulin⁺ retinal cells, which can be identified by their preferential β III-tubulin intensity
163 around the axonal base, are referred to as RGCs. Previous immunocytochemical analysis of these
164 cultures demonstrates that 60% of these retinal cells are neurons (neurofilament⁺/ β III-tubulin⁺),
165 of which 10% are Thy1⁺ RGCs (Suggate et al., 2009).

166 **2.4 *In vivo* experimental design**

167 Twenty female Sprague-Dawley rats (40 eyes) weighing at 200-220g (~8 weeks) were split into
168 8 groups (5 eyes per group) based on our previous *a priori* power calculations (Mead et al.,
169 2014). One group was left intact while the other 7 groups received an optic nerve crush (ONC)
170 on day 0. Intravitreal injection of AAV was given 7 days prior to ONC/day 0 and the experiment
171 finished on day 21. Electroretinography (ERG) and optical coherence tomography (OCT)
172 recording were also done 7 days prior to ONC/day 0 as well as on day 20.

173 **2.5 Optic nerve crush**

174 Anaesthesia was induced with 5%/95% Isoflurane/O₂ (Baxter Healthcare Corp, Deerfield,
175 IL)/1.5L per minute and maintained at 3.5% throughout the procedure whilst analgesia was
176 provided *via* an intraperitoneal injection of Buprenorphine (0.3 mg/kg). Intraorbital ONC was
177 performed as previously described (Berry et al., 1996). Briefly, the optic nerve was surgically
178 exposed under the superior orbital margin and crushed using fine forceps 1 mm posterior to the

179 lamina cribrosa, taking care to separate the dura mater and under lying retinal artery before
180 crushing.

181 **2.6 Intravitreal injection**

182 All virus collections (**Table 2**) were delivered at a concentration of 1×10^{11} vg/ml and in a final
183 volume of 5 μ l in sterile PBS, 0.001% pluronic, 7 days prior to ONC. Intravitreal injections,
184 posterior to the limbus, were performed under isoflurane-induced anaesthesia (described above)
185 using a pulled glass micropipette, produced from a glass capillary rod (Harvard Apparatus, Kent,
186 UK) using a Flaming-Brown micropipette puller (Sutter Instruments, Novato, CA, USA) with
187 care taken not to damage the lens.

188 **2.7 Confirmation of AAV-miRNA expression**

189 Each AAV expressing Hsa-mir-17, Hsa-mir-30c-2 and Hsa-mir-92a-1 coexpressed with EGFP
190 was intravitreally injected to the left eye of a rat. The right eye was used as the control by
191 injecting PBS. Two weeks later, the retina was dissected and efficiency of transduction was
192 confirmed following the EGFP expression. Total RNA were isolated and served for cDNA
193 synthesis and Q-PCR analysis to analyze the expression of each miRNA.

194 Three AAV expressing Hsa-mir-17, Hsa-mir-30c-2 or Hsa-mir-92a-1 were selected for the
195 confirmation of miRNA expression. Corresponding AAV were intravitreally injected into the left
196 eye, while the right eye, injected with PBS, was used as the control. Two weeks later, the retina
197 was dissected, and efficiency of transduction was confirmed following the EGFP expression.

198 Total small RNA was isolated from the retina using the mirVana miRNA isolation kit (Thermo
199 Fisher Scientific). The quality of isolated small RNA and the absence of large RNA
200 contamination were validated using a Bioanalyzer 2100 (Agilent). Total small RNA was used as

201 a template for cDNA synthesis. cDNA synthesis and Q-PCR analysis were performed using
202 miRCURY LNA miRNA Custom PCR Assays (Qiagen). Each cDNA sample (retina injected
203 with PBS, Hsa-mir-17-AAV, Hsa-mir-30c-2-AAV or Hsa-mir-92a-1-AAV) was tested for Hsa-
204 mir-17, Hsa-mir-30c-2 and Hsa-mir-92a-1 expression by Q-PCR. Fold inductions of each
205 miRNA in AAV-injected retina versus PBS-injected retina were calculated based on Ct values.
206 Data normalization was performed using the amount of total small RNAs used for each Q-PCR
207 sample.

208 **2.8 Electroretinography**

209 ERG was recorded using the Espion Ganzfeld full field system (Diagnosys LLC, Lowell, MA) 7
210 days prior to ONC (baseline) and 20 days post-ONC. Rats were dark adapted for 12 hours
211 overnight and prepared for ERG recording under dim red light ($>630\text{nm}$). Anaesthesia was
212 induced with intraperitoneal injection of Ketamine (100 mg/kg; Putney Inc, Portland,
213 ME)/Xylazine (10 mg/kg; Lloyd Inc, Shenandoah, IA) and eyes dilated with tropicamide.
214 Scotopic flash ERG was recorded from $-5.5 \log(\text{cd s}) \text{m}^{-2}$ to $1.0 \log(\text{cd s}) \text{m}^{-2}$ in 0.5 log unit
215 increments and traces were analyzed using in built Espion software. Traces at a light intensity of
216 $-5.0 \log(\text{cd s}) \text{m}^{-2}$ were chosen for analysis as they produced a clean, unambiguous positive
217 scotopic threshold (pSTR) at approximately 100 ms after stimulus, of which the peak amplitude
218 was recorded. All readings and analysis were performed by an individual masked to the
219 treatment groups.

220 **2.9 Optical coherence tomography measurements of the retinal nerve fiber layer**

221 OCT was performed on rats under anaesthesia (Ketamine and Xylazine, as above) 7 days prior to
222 ONC (baseline) and 20 days post-ONC. A Spectralis HRA3 confocal scanning laser

223 ophthalmoscope (Heidelberg Engineering, Heidelberg, Germany) was used to image the retinal
224 nerve fiber layer (RNFL) surrounding the optic nerve head and in-built software segmented the
225 RNFL and quantified the thickness. Segmentation was manually adjusted when necessary (by an
226 individual masked to the treatment group) to prevent inclusion of blood vessels that populate the
227 RNFL.

228 **2.10 Tissue preparation**

229 At 21 days post-ONC, animals were sacrificed with CO₂ overdose and perfused intracardially
230 with 4% paraformaldehyde (PFA) in PBS. Eyes and optic nerves were dissected and immersion
231 fixed in 4% PFA in PBS for a further 2 hours at 4°C before cryoprotection in 10%, 20% and
232 30% sucrose solution in PBS for 24 hours and stored at 4°C. Eyes and optic nerves were
233 embedded using optimal cutting temperature embedding medium (VWR International Inc,
234 Bridgeport, NJ) in peel-away mold containers (VWR International Inc) by rapid freezing with
235 ethanol/dry ice before storage at -80°C. Eyes and optic nerves were sectioned on a CM3050S
236 cryostat microtome (Leica Microsystems Inc, Bannockburn, IL) at -22°C at a thickness of 20 µm
237 and 14 µm, respectively, and mounted on positively charged glass slides (Superfrost Plus,
238 Thermo Fisher Scientific). Parasagittal eye and optic nerve sections were left to dry onto slides
239 overnight at 37°C before storage at -20°C. To ensure RGC counts were taken in the same plane,
240 eye sections were chosen with the optic nerve head visible.

241 **2.11 Immunocytochemistry**

242 Retinal cultures were fixed in 4% PFA in PBS for 10 minutes, washed for 3 x 10 minutes of
243 PBS, blocked in blocking solution (3% bovine serum albumin (g/ml), 0.1% Triton X-100 in
244 PBS) for 20 minutes and incubated with primary antibody (βIII-tubulin, 1:500, Sigma, #T-8660))

245 diluted in antibody diluting buffer (ADB; 0.5% bovine serum albumin, 0.3% Tween-20 in PBS)
246 for 1 hour at room temperature. Cultures were washed for 3 x 10 minutes in PBS, incubated with
247 the secondary antibody (Mouse IgG 488, 1:400, ThermoFisher, #A-11001) diluted in ADB for 1
248 hour at room temperature, washed for 3 x 10 minutes in PBS, mounted in Vectorshield mounting
249 medium containing DAPI (Vector Laboratories) and stored at 4°C.

250 **2.12 Immunohistochemistry**

251 Mounted tissue sections were equilibrated to room temperature, washed in PBS for 2 x 5
252 minutes, permeabilised in 0.1% Triton x-100 in PBS for 20 minutes and washed for 2 x 5
253 minutes in PBS. Sections were blocked in blocking buffer (75 µl; 0.5% bovine serum albumin
254 (g/ml), 0.3% Tween-20, 15% normal goat/donkey serum (Vector Laboratories) in PBS) in a
255 humidified chamber for 30 minutes and incubated with primary antibody (RNA-binding protein
256 with multiple splicing (RBPMS), 1:500, ThermoFisher, #ABN-1376; growth associated protein-
257 43 (GAP-43), 1:400, ThermoFisher, #33-5000; AAV, 1:200, ThermoFisher, #AB-PA1-4106)
258 diluted in ADB (15% normal goat serum in place of bovine serum albumin) overnight at 4°C.
259 The following day, slides were washed for 3 x 5 minutes in PBS and incubated with secondary
260 antibody (Mouse IgG 488, 1:400, ThermoFisher, #A11001; Guinea Pig IgG 546, 1:400,
261 ThermoFisher, #A-11074) diluted in ADB for 1 hour at room temperature. Slides were washed
262 for 3 x 5 minutes in PBS, mounted in Vectorshield mounting medium containing DAPI (Vector
263 Laboratories) and stored at 4°C before microscopic analysis. Negative controls including
264 omission of primary antibody were included in each run and were used to set the background
265 threshold levels prior to image capture.

266 **2.13 Microscopy and analysis**

267 All fluorescently stained sections were analysed by an operator blinded to the treatment groups.
268 For immunocytochemistry, wells were divided into 40 equal boxes and 12 were selected at
269 random. β III-tubulin⁺ retinal cells (identified by their staining morphology and referred to from
270 here on as RGCs), with or without neurites, were counted in each selected box. Fluorescently
271 stained cells were analysed using a Zeiss Z1 epifluorescence microscope (Carl Zeiss Inc,
272 Thornwood, NY). Neurite outgrowth was measured by dividing the well into 9 equal sectors and
273 the length of the longest neurite of each RGC in each sector was measured using Axiovision
274 software (Carl Zeiss Inc). All *in vitro* experiments were run in triplicate from pooled retinae from
275 2 animals and repeated on three independent occasions (total of 6 separate animals).

276 For immunohistochemistry of retina, RBPMS⁺ RGCs were counted in 20 μ m-thick sections
277 (imaged using a Zeiss LSM 700 confocal laser-scanning microscope) along a 250 μ m linear
278 region of the ganglion cell layer (GCL) either side of the optic nerve as previously described
279 (Mead et al., 2014). Six sections per retina and 5 retinae (from 5 different animals) per treatment
280 group were quantified. For immunohistochemistry of the optic nerve, GAP-43⁺ axons were
281 counted in 14 μ m thick longitudinal sections, imaged using a Zeiss LSM 700 confocal laser-
282 scanning microscope and image composites created using Photoshop CS6 (Adobe Systems, Inc.,
283 San Jose, CA). Note that GFP staining was only present in the RGC soma, not the axon. The
284 number of axons were quantified at 100, 200 and 500 μ m distance intervals extending proximal
285 and distal to the laminin⁺ crush site. Three sections per optic nerve and 5 optic nerves (from 5
286 different animals) per treatment group were quantified. The diameter of the nerve was measured
287 at each distance to determine the number of axons/mm width. This value was then used to derive
288 $\sum ad$, the total number of axons extending distance d in an optic nerve with radius r using:

289
$$\Sigma ad = \pi r^2 \times \frac{\text{average number of axons/mm width}}{\text{section thickness (0.015 mm)}}$$

290 **2.14 Statistics**

291 Animal numbers were determined beforehand using a power calculation (Faul et al., 2007; Mead
292 et al., 2014). All statistical tests were performed using SPSS 17.0 (IBM SPSS, Inc., Chicago, IL)
293 and data presented as mean \pm standard error of the mean (SEM) with graphs constructed using
294 Graphpad Prism (La Jolla, CA). Normal distribution was verified by Shapiro-Wilkes test prior to
295 parametric testing using a one-way analysis of variance (ANOVA) with a Tukey *post-hoc* test.
296 Statistical differences were considered significant at p values <0.05.

297 **3. Results**

298 Six miRNAs were selected for testing their therapeutic efficacy. Their selection was based on
299 their abundance in neuroprotective BMSC-derived sEV versus lower abundance in fibroblast-
300 derived sEV. Several of the selected miRNAs (miR-26a, miR-17-5p, miR-92a) were implicated
301 in the down-regulation of PTEN expression (Ding et al., 2017; Li and Yang, 2012; Zhang et al.,
302 2014) and PTEN knockdown was shown to promote RGC neuroprotection and axon regeneration
303 after ONC (Park et al., 2008). Instead of testing the miRNA individually, we combined three
304 miRNA into one AAV collection with a total of 5 different collections/AAV treatments (**Table**
305 **2**). RGCs, like other cells, can be transduced by multiple viral particles. Based on the number of
306 viral particles (5×10^8) and the number of RGCs in a Sprague Dawley rat (82818 ± 3949)
307 (Salinas-Navarro et al., 2009), there are approximately 6000 particles available per RGC. The
308 actual value is likely considerably lower as it assumes AAV2 is 100% preferential towards the
309 transduction of RGCs and no other retinal cells. Despite this, AAV staining confirms the

310 presence of multiple AAV molecules present per RGC (Figure. 2C) strongly indicating RGCs are
311 transduced by all three miRNA.

312 **3.1 Viral delivery of miRNA promotes a trend towards RGC** 313 **neuroprotection/neuritogenesis in mixed primary retinal cultures**

314 Mixed primary retinal cultures infected with different recombinant AAV were used to test
315 neuroprotective effects of miRNA *in vitro*. Cultures were kept for 3 days before analysis, in
316 which substantial loss of RGCs is expected. Control experiments showed that AAV2 virus
317 expressing GFP transduced $50.1 \pm 4.1\%$ of RGCs (β III tubulin⁺ cells) in retinal cultures (**Figure.**
318 **1E**).

319 Viral delivery of miRNA to these cultures elicited a non-significant trend towards RGC
320 neuroprotection with virus collection C and D promoting the highest (220.3 ± 17.4 , 220.6 ± 25.1
321 RGCs/well, respectively) followed by virus collection A, B and E (176.6 ± 20.1 , 196.1 ± 13.2 ,
322 212.4 ± 12.3 RGCs/well) in comparison to PBS and virus (GFP) treated controls (156.3 ± 10.5 ,
323 170.0 ± 21.1 RGCs/well; **Figure. 1A**).

324 Neuritogenesis was measured as the average length of the longest neurite (**Figure. 1B**). While
325 viral delivery of miRNA (virus collection A, B, C, D and E) trended towards a neuritogenic
326 effect (216.1 ± 60.3 , 217.1 ± 34.4 , 201.0 ± 30.9 , 226.6 ± 40.0 , 282.0 ± 50.0 μ m, respectively) in
327 comparison to PBS treated controls (126.4 ± 10.3 μ m), they did not in comparison to virus (GFP)
328 treated controls (192.1 ± 35.9 μ m). Virus (GFP) controls also trended to be more neuritogenic
329 than PBS treated controls. No statistically significant differences were seen.

330 **3.2 Viral delivery of miRNA *in vivo***

331 To confirm expression of miRNA after AAV transduction, four groups of RNA samples, from
332 total retina injected with PBS, hsa-mir-17-AAV, hsa-mir-30c-2-AAV and hsa-mir-92a-1-AAV,
333 were tested for each hsa-mir-17, hsa-mir-30c-2 and hsa-mir-92a-1 expression in separate Q-PCR
334 analysis. The injection of hsa-mir-17-AAV did not increase the amount of hsa-mir-17
335 (Supplementary Figure 1, left), while the injection of hsa-mir-92a-1 increased the amount of hsa-
336 mir-17. This shows that the hsa-mir-92a-1 may regulate hsa-mir-17 expression. The amount of
337 hsa-mir-30c-2-AAV (middle) and hsa-mir-92a-1 (right) were not changed by any of the tested
338 mir-AAV injection.

339 **3.3 Viral delivery of miRNA preserves RNFL thickness after ONC**

340 To test neuroprotective effects of miRNA *in vivo*, an ONC injury model was used with tissues
341 analysed 21 days post-crush. Control experiments demonstrated that AAV2 expressing GFP,
342 administered 7 days before the ONC, transduced $82.3 \pm 7.8\%$ RGCs after intravitreal injection in
343 our conditions (**Figure. 2A, B**).

344 The thickness of the RNFL was used as a measure of RGC axonal density (**Figure. 3**) and was
345 recorded as the mean \pm SEM (n=5), as were all subsequent *in vivo* endpoints. Measurements
346 were taken at 7 days before ONC and 20 days post-crush. RNFL thickness measurements
347 accurately correlate with the extent of RGC degeneration after ONC (Mead and Tomarev, 2016).
348 In untreated animals without ONC, RNFL thickness ($46.4 \pm 1.3 \mu\text{m}$) was no different from
349 baseline ($47.1 \pm 0.5 \mu\text{m}$; baseline was day 0 measurement from all animal groups). In animals
350 receiving virus collection A and C, RNFL thickness (25.8 ± 1.9 , $27.0 \pm 3.1 \mu\text{m}$, respectively) was
351 not significantly different from PBS and virus (GFP) treated control animals (24.0 ± 0.6 , $24.8 \pm$
352 $2.1 \mu\text{m}$, respectively). In contrast, in virus collection B, D and E treated animals, RNFL thickness

353 (34.3 ± 2.1, 37.0 ± 1.5, 36.0 ± 1.0 μm, respectively) was significantly higher than PBS and virus
354 (GFP) treated control animals.

355 **3.4 Viral delivery of miRNA promotes neuroprotection of RGCs following ONC**

356 ONC is characterised by the selective and rapid loss of RGCs. ONC (PBS and virus (GFP)
357 treated control) induced a significant loss of RBPMS⁺ RGCs by day 21 (4.7 ± 3.7 and 2.5 ±
358 0.5/mm of retina, respectively) compared to untreated controls without ONC (93.0 ± 7.8/mm of
359 retina; **Figure. 4**). While intravitreal delivery of virus collection A yielded no neuroprotective
360 effect (6.0 ± 0.6/mm of retina), virus collection B, C, D and E provided significant
361 neuroprotection of RBPMS⁺ RGCs (24.9 ± 14.2, 18.3 ± 3.4, 11.3 ± 2.7, 14.4 ± 1.5/mm of retina,
362 respectively) compared to PBS and virus (GFP) treated controls.

363 **3.5 Viral delivery of miRNA preserves RGC function**

364 The amplitude of the pSTR was used as a measure of RGC function, which (**Figure. 5**), which
365 deteriorates rapidly after ONC. Measurements were taken at 7 days before ONC and 20 days
366 post-crush. In PBS and virus (GFP) treated control animals, pSTR amplitude decreased
367 significantly (15.7 ± 7.4, 13.5 ± 5.9 μv, respectively) compared to untreated animals without
368 ONC (62.4 ± 16.0 μv). While intravitreal delivery of virus collection A, C and E yielded no
369 significant preservation of pSTR amplitude (13.9 ± 7.3, 24.4 ± 6.2, 19.3 ± 4.3 μv, respectively),
370 virus collection B and D significantly preserved pSTR amplitude (34.5 ± 4.4, 36.0 ± 8.0 μv,
371 respectively) compared to PBS and virus (GFP) treated controls.

372 **3.6 Viral delivery of miRNA promotes limited sprouting/protection of RGC axons,** 373 **but not regeneration**

374 Axons attempt, but ultimately fail to regenerate in animals after ONC, and this is amenable to
375 candidate axogenic treatments. No significant long-distance axon regeneration beyond the crush
376 site was observed in the experimental groups tested at day 21 (**Figure. 6**). Proximal to the crush
377 site, virus collection B, D, and E treatment yielded more GAP-43⁺ axons at 500 μm ($1010.2 \pm$
378 54.2 , 413.0 ± 48.7 , 923.2 ± 48.5 axons, respectively), 200 μm (938.0 ± 49.6 , 309.5 ± 41.4 , 816.0
379 ± 39.9 axons, respectively), and 100 μm (553.2 ± 39.7 , 184.5 ± 28.4 , 492.0 ± 31.2 axons,
380 respectively) as well as at the crush site (290.0 ± 29.9 , 66.9 ± 18.5 , 227.0 ± 26.7 axons,
381 respectively) in comparison to virus (GFP) treated controls (93.3 ± 15.9 , 81.3 ± 11.8 , $50.9 \pm$
382 10.5 , 53.8 ± 11.4 axons, respectively). Distal to the laminin⁺ crush site, the number of axons was
383 significantly higher only after virus collection B treatment and only at 100 μm from the crush
384 site (76.1 ± 27.9 axons) compared to virus (GFP) treated controls (24.4 ± 8.1 axons).

385 **3.7 Viral delivery of selective miRNA promoted downregulation of PTEN**

386 Many of the delivered miRNA target PTEN including miR-26a (Ding et al., 2017), miR-17-5p
387 (Dhar et al., 2015; Li and Yang, 2012), and miR-92a (Ke et al., 2015; Lu et al., 2017; Serr et al.,
388 2016; Xiao et al., 2017; Zhang et al., 2014), discussed further below. Immunohistochemical
389 staining of retinal sections demonstrated that PTEN immunofluorescence was qualitatively
390 reduced after treatment with virus collection B and D in comparison to virus (GFP) delivery
391 (**Figure. 7**).

392 **3.8 Predicted targets of miRNA**

393 Utilizing Ingenuity Pathway Analysis, we analyzed the targets of the 6 miRNA we delivered.
394 Since each miRNA is a stem loop that is broken into two mature miRNA, a 5p and 3p copy,
395 mRNA targeting was performed for all 12 mature miRNA. In total we found 6818 predicted

396 mRNA targets, 5815 targets that are present in both rat and human, 1551 of these which are
397 highly predicted, and 189 of these which have been experimentally observed (**Figure. 8**). Many
398 of these proteins are related to survival and regeneration and include Bcl proteins, STAT3, and
399 PTEN. In particular, PTEN was an experimentally observed target to three of the miRNA: miR-
400 26a-5p, miR-17-5p, and miR-92a-3p. Note that while all 12 of the miRNA have predicted
401 targeting information, only 7 have experimentally observed targets.

402 **4. Discussion**

403 The purpose of this study was to test neuroprotective and axogenic properties of six candidate
404 miRNAs that have been previously identified as more abundant in BMSC-sEV than in fibroblast
405 sEV (Mead et al., 2016; Mead and Tomarev, 2017).

406 Various combinations of these miRNAs were preferentially expressed in the RGCs of adult rats
407 using an AAV2 viral vector. AAV serotypes have varying preference for cell types with AAV2
408 being the optimal serotype for delivery into RGCs. AAV2 transduces approximately 85% of
409 RGCs after delivery into the vitreous body (Harvey et al., 2002; Martin et al., 2003). Comparable
410 efficacy was also observed in our experiments with all viruses confirmed to transduce >80% of
411 RGCs *in vivo* in the present study (**Figure. 2**). Previous studies using BAX knockout mice
412 suggest that transduction is still possible in RGCs injured by ONC (Nickells et al., 2017), we
413 decided to transduce 1 week prior to the ONC as it has been shown that AAV2-GFP takes 1
414 week before optimal *in vivo* expression is seen in RGCs (Smith and Chauhan, 2018). The
415 relatively short amount of time between injection of AAV and *in vivo* expression is a
416 consequence of our use of self-complementary AAV, which do not require host cell second
417 strand synthesis, a significant rate-limiting step (McCarty, 2008). Intravitreal delivery of AAV2

418 shows no detrimental effects on RGCs, as measured by ERG (pSTR and nSTR) as well as OCT
419 (RNFL) (Smith and Chauhan, 2018). While we could not confirm the over expression of every
420 miRNA, likely due to the high endogenous expression already present in retinal tissue, AAV-
421 mir-92a-1 led to a trend towards mir-92a-1 over expression and significant overexpression of
422 mir-17. It is important to highlight that Q-PCR was done on total retina whereas AAV
423 preferentially transduced RGC and is thus a likely reason for our inability to demonstrate
424 significant differences in miRNA. We were still able to detect some differences however as well
425 as PTEN reductions, demonstrating that AAV-miRNA was exerting a biological effect.

426 The ability of miRNA to downregulate a multitude of different mRNA(Gebert and MacRae,
427 2018) makes them a strong candidate as non-synthetic neuroprotective treatments for RGCs.
428 They can be easily delivered into the vitreous to provide an immediate and direct effect on
429 RGCs, although this avenue of research, utilizing miRNA as a treatment in the eye, is still poorly
430 studied in the literature(Klingeborn et al., 2017). Delivery of miR-93-5p to RGCs in culture
431 provides neuroprotection from NMDA-induced death and this miRNA was chosen based on its
432 NMDA-induced downregulation (Li et al., 2018). Another miRNA downregulated in glaucoma
433 is miR-200a, based on RT-qPCR of retinal samples from wildtype and microbead-induced
434 glaucomatous mice (Peng et al., 2018). Intravenous injection of miR-200a mimics into a
435 microbead mouse model of glaucoma provides significant neuroprotection of RGCs as well as
436 preservation of RNFL thickness, likely through the knockdown of FGF7. A recent experiment
437 utilized 12-week DBA/2J mice that received an injection of glutamate to induce RGC
438 excitotoxicity. Intravitreal delivery of a virus expressing miR-141-3p led to a significant increase
439 in RGC survival along with downregulation of apoptotic signalling pathways such as Bax and
440 caspase-3 (Zhang et al., 2018).

441 A widely published target of many miRNA is PTEN (Bermúdez Brito et al., 2015), in large part
442 due to PTEN being a tumor suppressor protein implicated in a number of cancers (Chalhoub and
443 Baker, 2009). In the field of neuroregeneration and neuroprotection, PTEN knockdown
444 significantly promotes both (Berry et al., 2016; Park et al., 2008) *via* activation of the
445 mTOR/PI3K pathway. The treatment of RGCs in culture with the above mentioned miR-93-5p
446 promoted neuroprotection through its targeting of PTEN (Li et al., 2018).

447 Many of the candidate miRNAs used in the present experiment target PTEN including miR-26a,
448 demonstrated in gastric cancer cells (Ding et al., 2017), miR-17-5p, demonstrated in
449 glioblastoma cells (Li and Yang, 2012) and prostate cancer cells (Dhar et al., 2015), and miR-
450 92a, demonstrated in a variety of paradigms (Ke et al., 2015; Lu et al., 2017; Serr et al., 2016;
451 Xiao et al., 2017; Zhang et al., 2014). Delivery of virus collection B (miR-17-5p, miR-30c-2 and
452 miR-92a) and virus collection D (miR-92a, miR-292 and miR-182) promoted significant
453 neuroprotection, preservation of RNFL thickness as measured by OCT, and preservation of RGC
454 function, as measured by ERG. These effects coincided with a qualitative reduction in PTEN
455 immunofluorescence within the retina, in contrast to virus (GFP) controls where PTEN was
456 expressed in the GCL and inner nuclear layer. In virus collection B treated animals, the most
457 substantial neuroprotection of RGCs was seen alongside minor axonal sprouting. Given that
458 significant more axons were seen in this treatment group proximal to the lesion site in
459 comparison to virus (GFP) treated control, it is likely the effect is not on regeneration but on
460 preventing axonal degeneration. Nevertheless, the enhanced effect of virus collection B over D
461 can be explained by the presence of miR-17-5p and miR-30c-2 in virus collection B but not virus
462 collection D, which may target SOCS6 (Wu et al., 2014) and BCL9 (Jia et al., 2011), amongst
463 many other predicted targets. Interestingly these miRNA were expressed in virus collection A yet

464 showed no therapeutic effect, demonstrating that their combination with miR-92a is required to
465 elicit the positive effects seen. Virus collection A also contained miR-26a which targets GSK3 β ,
466 a kinase whose downregulation is expected to lead to CNS axon regeneration (Guo et al., 2016)
467 yet this was not observed in the present study. Virus collection E contained all 6 miRNAs yet did
468 not give the most pronounced effects with significance only seen for RNFL thickness and RGC
469 survival. It can be suggested that because virus collection E was a combination of 2 virus batches
470 each expressing 3 miRNAs, a competitive effect was observed leading to sub-threshold levels of
471 each miRNA being delivered. This hypothesis is demonstrated by the lack of PTEN
472 downregulation in virus collection E treated animals.

473 While the *in vitro* experiment demonstrated a trend towards neuroprotection/neuritogenesis, no
474 significant effects were seen. This could be explained by the shorter duration afforded for
475 successful transduction *in vitro* and the subsequently reduced transduction efficiency ($50.1 \pm$
476 4.1%) on RGCs that we observed (**Figure. 1**). We also noticed a trending neuritogenic effect by
477 AAV-GFP control in comparison to PBS control, suggesting the virus itself was having a
478 confounding effect on the results and promoting neuritogenesis irrespective of the miRNA. This
479 observation was not seen *in vivo*.

480 In conclusion we have demonstrated that virally delivered miRNA can significantly protect
481 RGCs and their axons from degeneration and dysfunction. The mechanism of action is likely
482 multifaceted, with several miRNA playing a role. PTEN, a confirmed target of many of the
483 delivered miRNA was qualitatively reduced and coincided with the therapeutic effects observed.
484 Further study is required to determine exactly which miRNA (and through which mRNA targets)
485 exert greatest therapeutic efficacy.

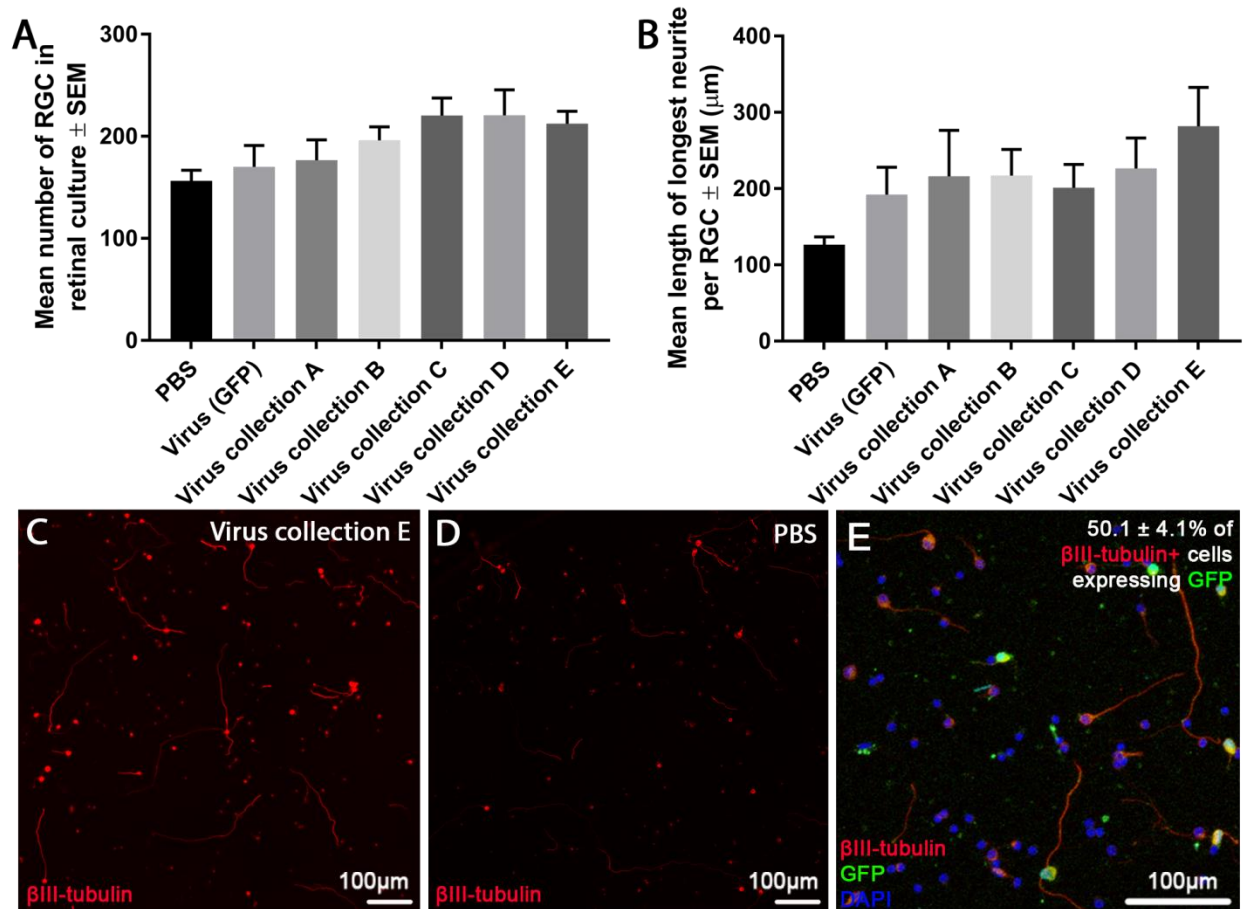
486 **5. Acknowledgements**

487 This work was supported by the Intramural Research Programs of the National Eye Institute.

488 This project has received funding from the European Union's Horizon 2020 research and

489 innovation programme under the Marie Skłodowska-Curie grant agreement No. 749346.

490



491

492 Figure 1: Effects of virally delivered miRNA on RGC neuroprotection/neuritogenesis in culture.

493 The number of surviving β III-tubulin⁺ RGCs (A) and the average length of their longest neurite

494 (B) in heterogeneous adult rat retinal cultures treated with different viruses are shown. No

495 significant differences between virus treated and virus (GFP) treated groups was seen.

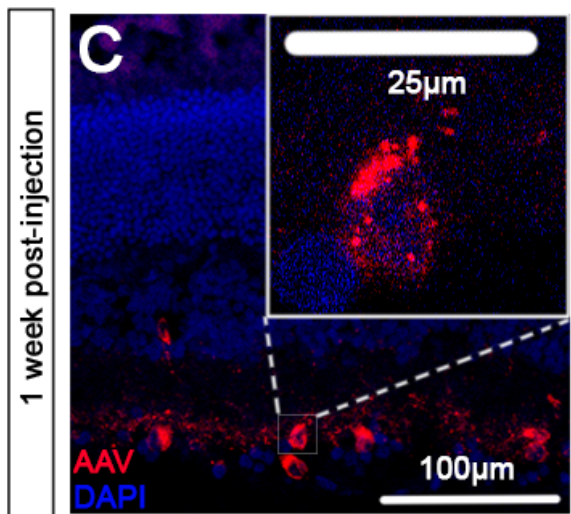
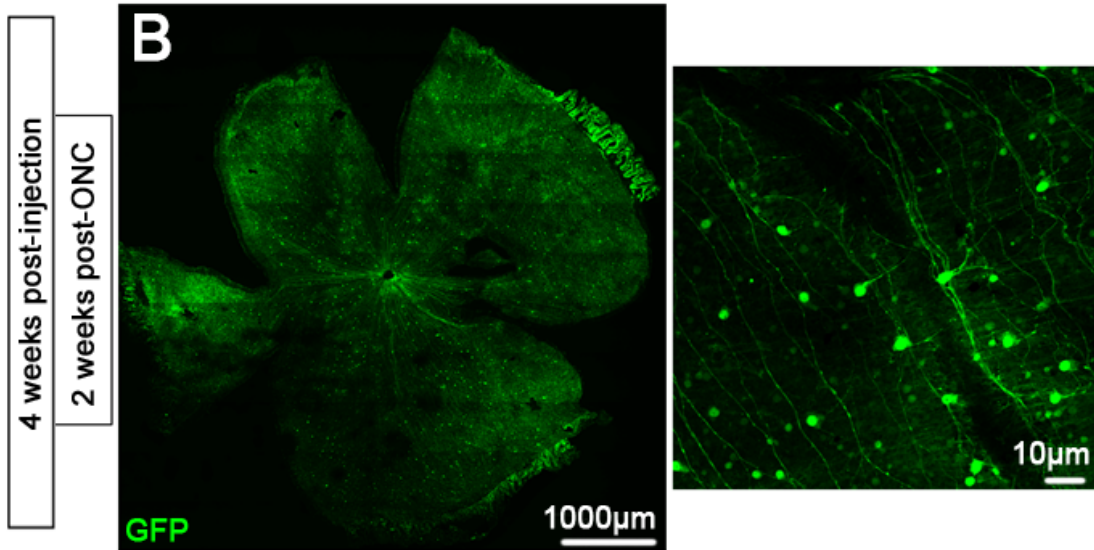
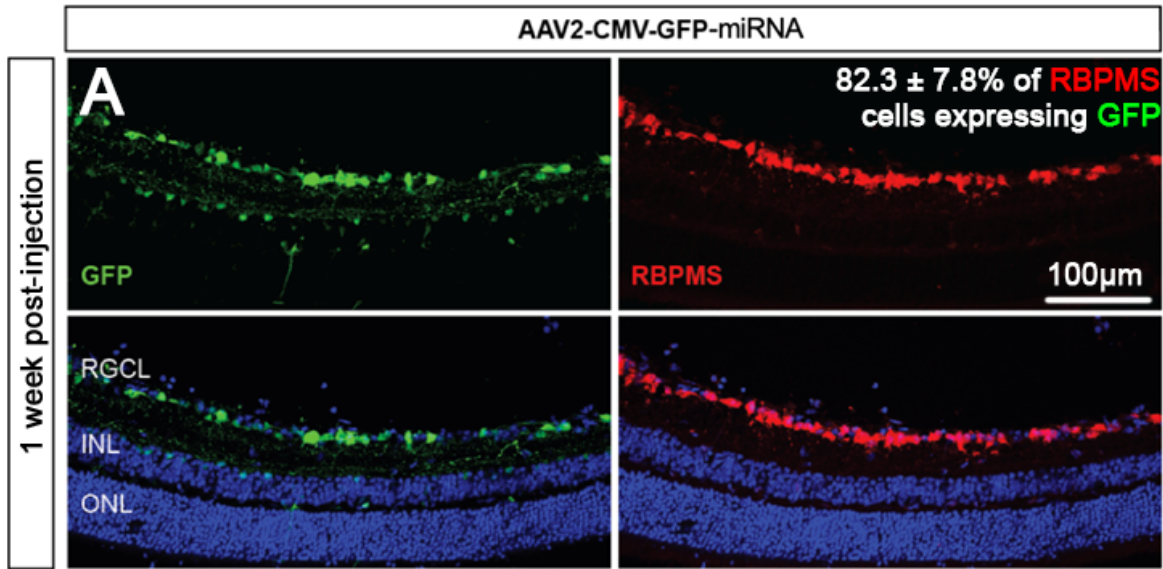
496 Representative images of retinal cultures treated with virus collection E (C) or PBS (D) are

497 shown. Finally, transduction efficiency is shown *via* representative *in vitro* retinal cultures 3 days

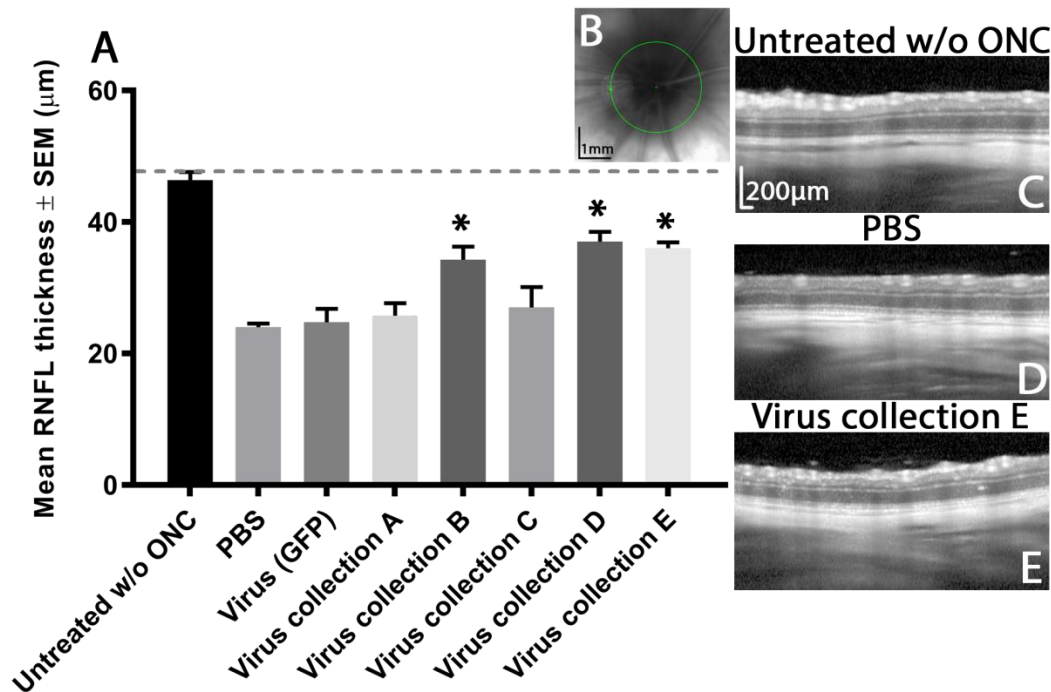
498 post-AAV2 treatment, counter stained with β III-tubulin (green) and DAPI (blue). Images are

499 representative of the 3 separate cultures/3 repeats per culture. Sections were stained with β III-

500 tubulin (red; scale bar: 100 μ m).

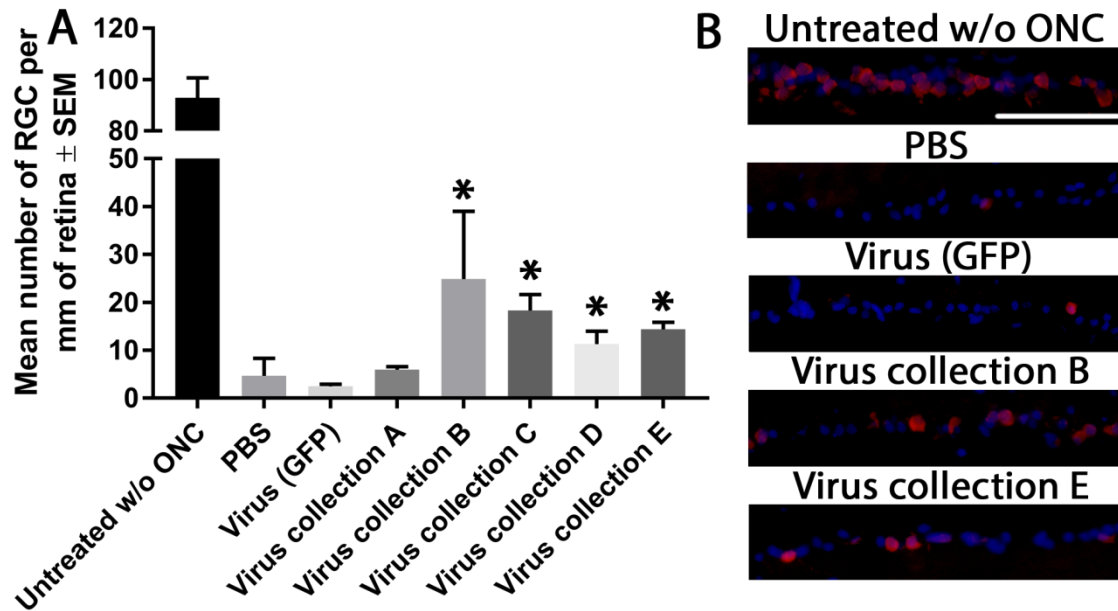


502 Figure 2: Retinal GFP expression. Representative images and transduction efficiency of retinal
 503 sections (A) and retinal wholemounts (B) treated with AAV2 virus expressing GFP (*green*).
 504 Retinal sections are from animals 1-week post-AAV2 injection and counterstained with RBPMS
 505 (red) whereas wholemounts are from animals 4-weeks post-AAV2 injection and 2 weeks post-
 506 optic nerve crush (ONC). Finally, retinal sections 1-week post-AAV2 injection stained for AAV
 507 are shown (C), with a magnified inset demonstrating the extent of transduction in a retinal
 508 ganglion cell. Retinal ganglion cell layer (RGCL), inner nuclear layer (INL), and outer nuclear
 509 layer (ONL) are labeled. Images representative of 5 animals per group.



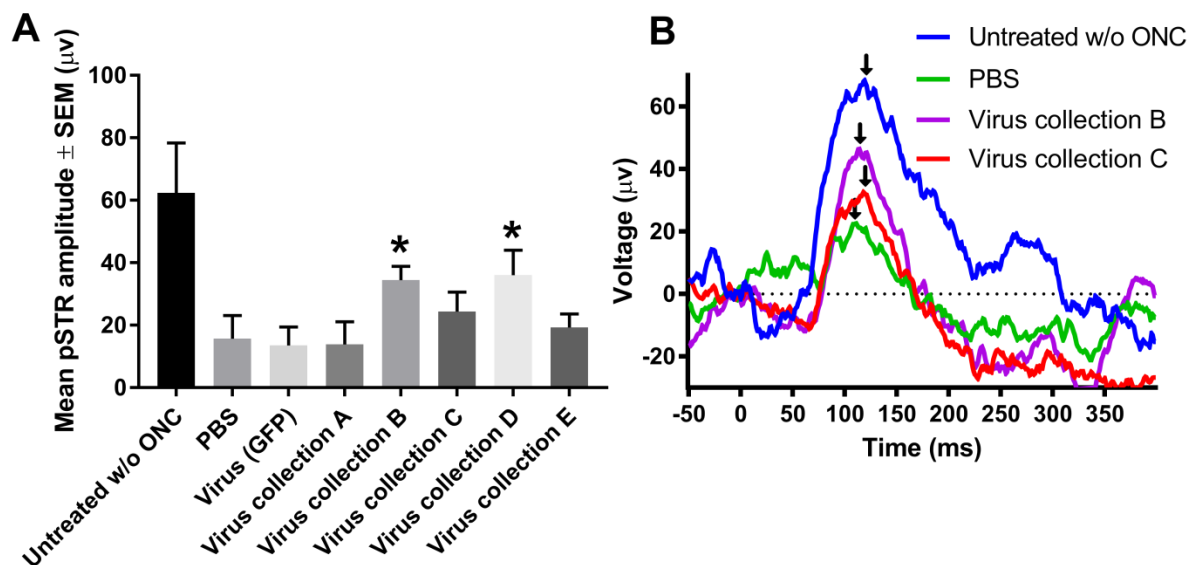
510

511 Figure 3: RNFL thickness after ONC. Graph depicting the mean average (\pm SEM) RNFL
 512 thickness (μm) of animals before (*dashed grey line*), and 21 days after ONC (A). *Asterisks*
 513 indicate significant differences ($p < 0.05$) from PBS and virus (GFP) control treated animals. To
 514 encapsulate the entirety of the RNFL as it courses towards the optic nerve head, measurements
 515 were recorded at this region (B; *scale bar 1 mm*) and representative images from the 5 animals
 516 per group are shown (C,D and E; *scale bars 200 μm*).



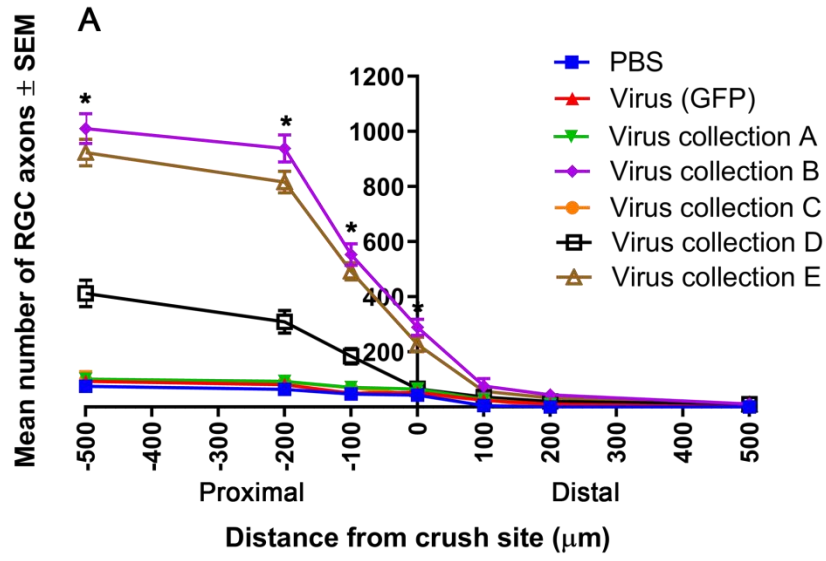
517

518 Figure 4: RBPMS⁺ RGC counts after ONC. Graph depicting the number of RBPMS⁺ RGCs (per
 519 mm or retina) 21 days after ONC (A). Asterisks indicate significant differences ($p < 0.05$) from
 520 PBS and virus (GFP) control treated animals. Representative images of the ganglion cell layer of
 521 retina stained for RBPMS (green) and DAPI (blue) from the 5 animals per groups are shown (B;
 522 scale bar 100 μ m)

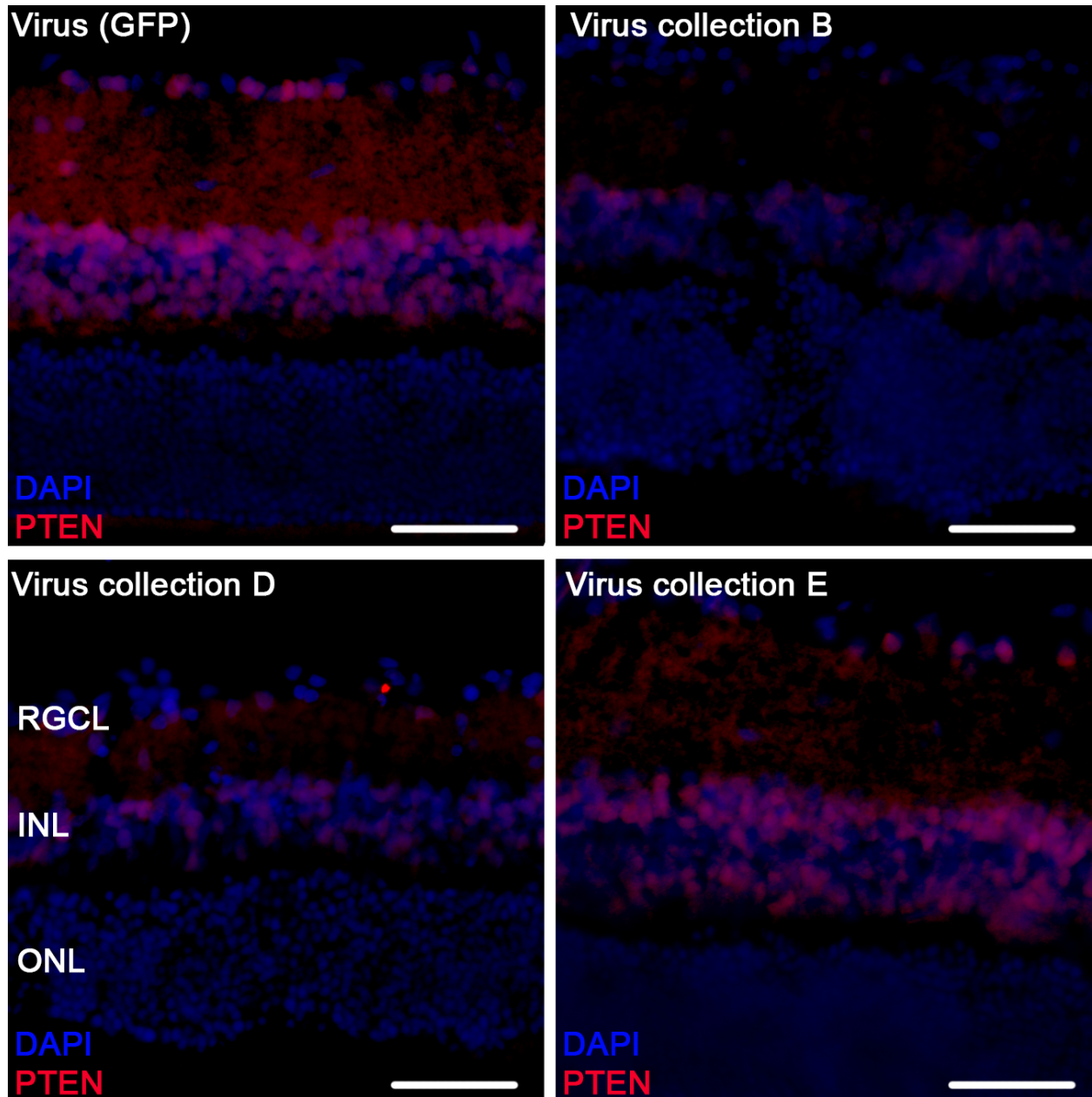


523

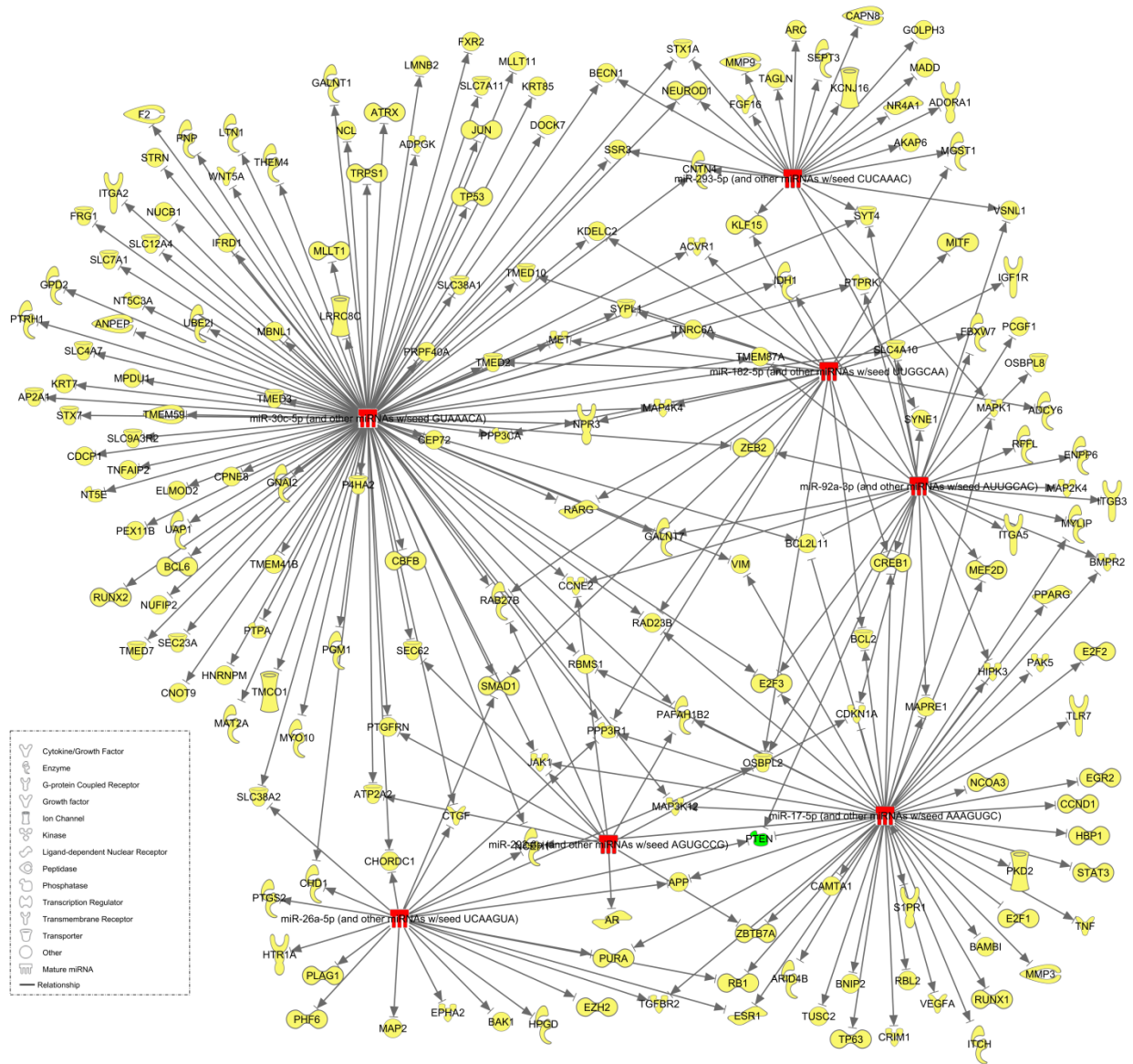
524 Figure 5: pSTR amplitude after ONC. Mean pSTR amplitude measured with ERG 21 days after
 525 ONC (A). Asterisks indicate significant differences ($p < 0.05$) from PBS and virus (GFP) control
 526 treated animals. Representative traces from the 5 animals per group are shown (B). Black arrows
 527 indicate peak amplitude that was recorded as the pSTR.



529 Figure 6: Protection against axonal degeneration in the optic nerve. Mean number of GAP-43⁺
530 axons at 100-500 μm distances proximal and distal to the laminin⁺ crush site (A). Asterisks
531 indicate significant differences ($p < 0.05$) from PBS and virus (GFP) control treated animals.
532 Representative image (from 5 animals) of an optic nerve from animals treated with virus B or
533 virus (GFP) control, immunohistochemically stained for laminin (red) and GAP-43 (yellow) are
534 shown (B; scale bar 100 μm).

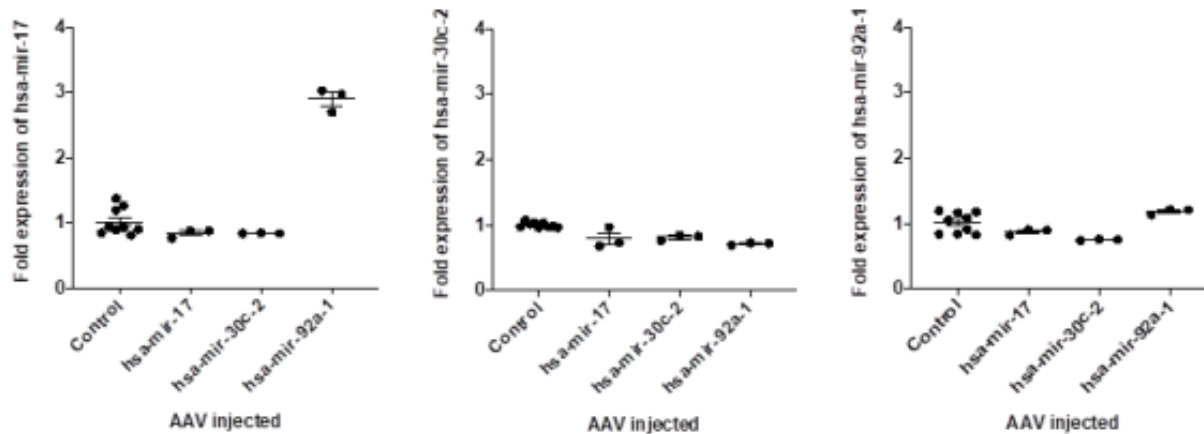


535
536 Figure 7: Retinal PTEN expression after ONC. Representative images of parasagittal retinal
537 sections stained for PTEN (red) and DAPI (blue), from 5 animals treated with virus (GFP)
538 control, virus B, virus D and virus E. Retinal ganglion cell layer (RGCL), inner nuclear layer
539 (INL), and outer nuclear layer (ONL) are labeled (scale bar 100 μm).



540

541 Figure 8: mRNA targets of delivered miRNA. Experimentally observed targets for virally
 542 delivered miRNA, obtained through Ingenuity Pathway Analysis software, are shown. Of the 6
 543 miRNA stem loops and subsequent 12 mature miRNA sequences, 7 (red) have experimentally
 544 observed targets totaling at 189 mRNA (yellow) which includes the confirmed knocked down
 545 target mRNA PTEN (green).



546

547 Supplementary Figure 1: Fold expression of miRNA. Fold change in the expression of Hsa-mir-
 548 17, Hsa-mir-30c-2 and Hsa-mir-92a-1 in four groups of retina injected with either PBS or AAV
 549 expressing Hsa-mir-17, Hsa-mir-30c-2 and Hsa-mir-92a-1. Data normalization was performed
 550 using the amount of total small RNAs used for each Q-PCR sample.

551

552 6. References

553 Bera, A., Das, F., Ghosh-Choudhury, N., Mariappan, M.M., Kasinath, B.S., Ghosh Choudhury, G., 2017.
 554 Reciprocal regulation of miR-214 and PTEN by high glucose regulates renal glomerular mesangial and
 555 proximal tubular epithelial cell hypertrophy and matrix expansion. *American Journal of Physiology - Cell*
 556 *Physiology* 313, C430-C447.

557 Bermúdez Brito, M., Goulielmaki, E., Papakonstanti, E.A., 2015. Focus on PTEN Regulation. *Frontiers in*
 558 *oncology* 5, 166-166.

559 Berry, M., Ahmed, Z., Morgan-Warren, P., Fulton, D., Logan, A., 2016. Prospects for mTOR-mediated
 560 functional repair after central nervous system trauma. *Neurobiol Dis* 85, 99-110.

561 Berry, M., Carlile, J., Hunter, A., 1996. Peripheral nerve explants grafted into the vitreous body of the
 562 eye promote the regeneration of retinal ganglion cell axons severed in the optic nerve. *J Neurocytol* 25,
 563 147-170.

564 Chalhoub, N., Baker, S.J., 2009. PTEN and the PI3-kinase pathway in cancer. *Annual review of pathology*
 565 *4*, 127-150.

566 Ching, R.C., Wiberg, M., Kingham, P.J., 2018. Schwann cell-like differentiated adipose stem cells promote
 567 neurite outgrowth via secreted exosomes and RNA transfer. *Stem Cell Research & Therapy* 9.

568 Dhar, S., Kumar, A., Rimando, A.M., Zhang, X., Levenson, A.S., 2015. Resveratrol and pterostilbene
 569 epigenetically restore PTEN expression by targeting oncomiRs of the miR-17 family in prostate cancer.
 570 *Oncotarget* 6, 27214-27226.

571 Ding, K., Wu, Z., Wang, N., Wang, X., Wang, Y., Qian, P., Meng, G., Tan, S., 2017. MiR-26a performs
 572 converse roles in proliferation and metastasis of different gastric cancer cells via regulating of PTEN
 573 expression. *Pathology - Research and Practice* 213, 467-475.

574 Faul, F., Erdfelder, E., Lang, A.G., Buchner, A., 2007. G*Power 3: a flexible statistical power analysis
 575 program for the social, behavioral, and biomedical sciences. *Behavior research methods* 39, 175-191.

576 Flachsbarth, K., Jankowiak, W., Kruszewski, K., Helbing, S., Bartsch, S., Bartsch, U., 2018. Pronounced
577 synergistic neuroprotective effect of GDNF and CNTF on axotomized retinal ganglion cells in the adult
578 mouse. *Experimental Eye Research* 176, 258-265.

579 Gebert, L.F.R., MacRae, I.J., 2018. Regulation of microRNA function in animals. *Nature Reviews*
580 *Molecular Cell Biology*.

581 Guo, X., Snider, W.D., Chen, B., 2016. GSK3 β regulates AKT-induced central nervous system axon
582 regeneration via an eIF2B ϵ -dependent, mTORC1-independent pathway. *eLife* 5, e11903-e11903.

583 Harvey, A.R., Kamphuis, W., Eggers, R., Symons, N.A., Blits, B., Niclou, S., Boer, G.J., Verhaagen, J., 2002.
584 Intravitreal Injection of Adeno-associated Viral Vectors Results in the Transduction of Different Types of
585 Retinal Neurons in Neonatal and Adult Rats: A Comparison with Lentiviral Vectors. *Molecular and*
586 *Cellular Neuroscience* 21, 141-157.

587 Hoye, M.L., Regan, M.R., Jensen, L.A., Lake, A.M., Reddy, L.V., Vidensky, S., Richard, J.-P., Maragakis, N.J.,
588 Rothstein, J.D., Dougherty, J.D., Miller, T.M., 2018. Motor neuron-derived microRNAs cause astrocyte
589 dysfunction in amyotrophic lateral sclerosis. *Brain* 141, 2561-2575.

590 Jia, W., Eneh, J.O., Ratnaparkhe, S., Altman, M.K., Murph, M.M., 2011. MicroRNA-30c-2* Expressed in
591 Ovarian Cancer Cells Suppresses Growth Factor-Induced Cellular Proliferation and Downregulates the
592 Oncogene BCL9. *Molecular Cancer Research* 9, 1732.

593 Johnson, T.V., Bull, N.D., Hunt, D.P., Marina, N., Tomarev, S.I., Martin, K.R., 2010. Neuroprotective
594 Effects of Intravitreal Mesenchymal Stem Cell Transplantation in Experimental Glaucoma. *Investigative*
595 *Ophthalmology & Visual Science* 51, 2051-2059.

596 Juźwik, C.A., Drake, S., Lécuyer, M.-A., Johnson, R.M., Morquette, B., Zhang, Y., Charabati, M., Sagan,
597 S.M., Bar-Or, A., Prat, A., Fournier, A.E., 2018. Neuronal microRNA regulation in Experimental
598 Autoimmune Encephalomyelitis. *Scientific Reports* 8, 13437.

599 Ke, T.-W., Wei, P.-L., Yeh, K.-T., Chen, W.T.-L., Cheng, Y.-W., 2015. MiR-92a Promotes Cell Metastasis of
600 Colorectal Cancer Through PTEN-Mediated PI3K/AKT Pathway. *Annals of Surgical Oncology* 22, 2649-
601 2655.

602 Klingeborn, M., Dismuke, W.M., Rickman, C.B., Stamer, W.D., 2017. Roles of Exosomes in the Normal
603 and Diseased Eye. *Progress in retinal and eye research* 59, 158-177.

604 Kole, C., Klipfel, L., Yang, Y., Ferracane, V., Blond, F., Reichman, S., Millet-Puel, G., Clérin, E., Aït-Ali, N.,
605 Pagan, D., Camara, H., Delyfer, M.-N., Nandrot, E.F., Sahel, J.-A., Goureau, O., Léveillard, T., 2018.
606 *Otx2*-Genetically Modified Retinal Pigment Epithelial Cells Rescue Photoreceptors after
607 Transplantation. *Mol Ther* 26, 219-237.

608 Li, H., Yang, B.B., 2012. Stress response of glioblastoma cells mediated by miR-17-5p targeting PTEN and
609 the passenger strand miR-17-3p targeting MDM2. *Oncotarget* 3, 1653-1668.

610 Li, R., Jin, Y., Li, Q., Sun, X., Zhu, H., Cui, H., 2018. MiR-93-5p targeting PTEN regulates the NMDA-induced
611 autophagy of retinal ganglion cells via AKT/mTOR pathway in glaucoma. *Biomedicine &*
612 *Pharmacotherapy* 100, 1-7.

613 Liu, J., Carmell, M.A., Rivas, F.V., Marsden, C.G., Thomson, J.M., Song, J.-J., Hammond, S.M., Joshua-Tor,
614 L., Hannon, G.J., 2004. Argonaute2 Is the Catalytic Engine of Mammalian RNAi. *Science* 305, 1437-1441.

615 Logan, A., Ahmed, Z., Baird, A., Gonzalez, A.M., Berry, M., 2006. Neurotrophic factor synergy is required
616 for neuronal survival and disinhibited axon regeneration after CNS injury. *Brain* 129, 490-502.

617 Lu, C.J., Shan, Z.X., Hong, J., Yang, L.X., 2017. MicroRNA-92a promotes epithelial-mesenchymal transition
618 through activation of PTEN/PI3K/AKT signaling pathway in non-small cell lung cancer metastasis. *Int J*
619 *Oncol* 51, 235-244.

620 Martin, K.R.G., Quigley, H.A., Zack, D.J., Levkovitch-Verbin, H., Kielczewski, J., Valenta, D., Baumrind, L.,
621 Pease, M.E., Klein, R.L., Hauswirth, W.W., 2003. Gene Therapy with Brain-Derived Neurotrophic Factor
622 As a Protection: Retinal Ganglion Cells in a Rat Glaucoma Model. *Investigative Ophthalmology & Visual*
623 *Science* 44, 4357-4365.

624 McCarty, D.M., 2008. Self-complementary AAV Vectors; Advances and Applications. *Mol Ther* 16, 1648-
625 1656.

626 Mead, B., Amaral, J., Tomarev, S., 2018. Mesenchymal Stem Cell-Derived Small Extracellular Vesicles
627 Promote Neuroprotection in Rodent Models of Glaucoma. *Investigative Ophthalmology & Visual Science*
628 59, 702-714.

629 Mead, B., Hill, L.J., Blanch, R.J., Ward, K., Logan, A., Berry, M., Leadbeater, W., Scheven, B.A., 2016.
630 Mesenchymal stromal cell-mediated neuroprotection and functional preservation of retinal ganglion
631 cells in a rodent model of glaucoma. *Cytotherapy* 18, 487-496.

632 Mead, B., Logan, A., Berry, M., Leadbeater, W., Scheven, B.A., 2013. Intravitreally transplanted dental
633 pulp stem cells promote neuroprotection and axon regeneration of retinal ganglion cells after optic
634 nerve injury. *Invest Ophthalmol Vis Sci* 54, 7544-7556.

635 Mead, B., Thompson, A., Scheven, B.A., Logan, A., Berry, M., Leadbeater, W., 2014. Comparative
636 evaluation of methods for estimating retinal ganglion cell loss in retinal sections and wholemounts. *Plos*
637 *One* 9, e110612.

638 Mead, B., Tomarev, S., 2016. Evaluating retinal ganglion cell loss and dysfunction. *Exp Eye Res* 151, 96-
639 106.

640 Mead, B., Tomarev, S., 2017. BMSC-derived exosomes promote survival of retinal ganglion cells through
641 miRNA-dependent mechanisms. *Stem cells translational medicine* 6, 1273-1285.

642 Nickells, R.W., Schmitt, H.M., Maes, M.E., Schlamp, C.L., 2017. AAV2-Mediated Transduction of the
643 Mouse Retina After Optic Nerve Injury. *Investigative Ophthalmology & Visual Science* 58, 6091-6104.

644 Nie, X.-G., Fan, D.-S., Huang, Y.-X., He, Y.-Y., Dong, B.-L., Gao, F., 2018. Downregulation of microRNA-149
645 in retinal ganglion cells suppresses apoptosis through activation of the PI3K/Akt signaling pathway in
646 mouse with glaucoma. *American Journal of Physiology-Cell Physiology*.

647 Osborne, A., Khatib, T.Z., Songra, L., Barber, A.C., Hall, K., Kong, G.Y.X., Widdowson, P.S., Martin, K.R.,
648 2018. Neuroprotection of retinal ganglion cells by a novel gene therapy construct that achieves
649 sustained enhancement of brain-derived neurotrophic factor/tropomyosin-related kinase receptor-B
650 signaling. *Cell Death & Disease* 9, 1007.

651 Park, K.K., Liu, K., Hu, Y., Smith, P.D., Wang, C., Cai, B., Xu, B., Connolly, L., Kramvis, I., Sahin, M., He, Z.,
652 2008. Promoting Axon Regeneration in the Adult CNS by Modulation of the PTEN/mTOR Pathway.
653 *Science* 322, 963-966.

654 Peng, H., Sun, Y.-B., Hao, J.-L., Lu, C.-W., Bi, M.-C., Song, E., 2018. Neuroprotective effects of
655 overexpressed microRNA-200a on activation of glaucoma-related retinal glial cells and apoptosis of
656 ganglion cells via downregulating FGF7-mediated MAPK signaling pathway. *Cellular Signalling*.

657 Rajgor, D., 2018. Macro roles for microRNAs in neurodegenerative diseases. *Non-coding RNA Research*
658 3, 154-159.

659 Salinas-Navarro, M., Mayor-Torroglosa, S., Jimenez-Lopez, M., Aviles-Trigueros, M., Holmes, T.M., Lund,
660 R.D., Villegas-Perez, M.P., Vidal-Sanz, M., 2009. A computerized analysis of the entire retinal ganglion
661 cell population and its spatial distribution in adult rats. *Vision Res* 49, 115-126.

662 Sayed, D., He, M., Hong, C., Gao, S., Rane, S., Yang, Z., Abdellatif, M., 2010. MicroRNA-21 Is a
663 Downstream Effector of AKT That Mediates Its Antiapoptotic Effects via Suppression of Fas Ligand. *The*
664 *Journal of biological chemistry* 285, 20281-20290.

665 Serr, I., Fürst, R.W., Ott, V.B., Scherm, M.G., Nikolaev, A., Gökmen, F., Kälin, S., Zillmer, S., Bunk, M.,
666 Weigmann, B., Kunschke, N., Loretz, B., Lehr, C.-M., Kirchner, B., Haase, B., Pfaffl, M., Waisman, A.,
667 Willis, R.A., Ziegler, A.-G., Daniel, C., 2016. miRNA92a targets KLF2 and the phosphatase PTEN signaling
668 to promote human T follicular helper precursors in T1D islet autoimmunity. *Proceedings of the National*
669 *Academy of Sciences* 113, E6659-E6668.

670 Smith, C.A., Chauhan, B.C., 2018. In vivo imaging of adeno-associated viral vector labelled retinal
671 ganglion cells. *Scientific Reports* 8, 1490.

672 Suggate, E.L., Ahmed, Z., Read, M.L., Eaton-Charnock, K., Douglas, M.R., Gonzalez, A.M., Berry, M.,
673 Logan, A., 2009. Optimisation of siRNA-mediated RhoA silencing in neuronal cultures. *Molecular and*
674 *Cellular Neuroscience* 40, 451-462.

675 Wang, X., Zhang, X., Ren, X.-P., Chen, J., Liu, H., Yang, J., Medvedovic, M., Hu, Z., Fan, G.-C., 2010.
676 MicroRNA-494 Targeting both Pro-apoptotic and Anti-apoptotic Proteins Protects against
677 Ischemia/Reperfusion-Induced Cardiac Injury. *Circulation* 122, 1308-1318.

678 Wu, Q., Luo, G., Yang, Z., Zhu, F., An, Y., Shi, Y., Fan, D., 2014. miR-17-5p promotes proliferation by
679 targeting SOCS6 in gastric cancer cells. *FEBS Letters* 588, 2055-2062.

680 Xia, X.W., Li, Y., Wang, W.B., Tang, F., Tan, J., Sun, L.Y., Li, Q.H., Sun, L., Tang, B., He, S.Q., 2015.
681 MicroRNA-1908 functions as a glioblastoma oncogene by suppressing PTEN tumor suppressor pathway.
682 *Mol Cancer* 14.

683 Xiao, J., Yu, W.F., Hu, K.Z., Li, M.Q., Chen, J.W., Li, Z.C., 2017. miR-92a promotes tumor growth of
684 osteosarcoma by targeting PTEN/AKT signaling pathway. *Oncol Rep* 37, 2513-2521.

685 Zhang, G., Zhou, H., Xiao, H., Liu, Z., Tian, H., Zhou, T., 2014. MicroRNA-92a Functions as an Oncogene in
686 Colorectal Cancer by Targeting PTEN. *Digestive Diseases and Sciences* 59, 98-107.

687 Zhang, L.-Q., Cui, H., Yu, Y.-B., Shi, H.-Q., Zhou, Y., Liu, M.-J., 2018. MicroRNA-141-3p inhibits retinal
688 neovascularization and retinal ganglion cell apoptosis in glaucoma mice through the inactivation of
689 Docking protein 5-dependent mitogen-activated protein kinase signaling pathway. *Journal of cellular*
690 *physiology* 0.

691 Zhang, Y., Chopp, M., Liu, X.S., Katakowski, M., Wang, X., Tian, X., Wu, D., Zhang, Z.G., 2016. Exosomes
692 Derived from Mesenchymal Stromal Cells Promote Axonal Growth of Cortical Neurons. *Mol Neurobiol.*

693

694